

## Monitoring land deformation in Changzhou city (China) with multi-band InSAR data sets from 2006 to 2012

Yanyan Lu, Chang-Qing Ke, Xiaobing Zhou, Manman Wang, Hui Lin, Deliang Chen & Houjun Jiang

To cite this article: Yanyan Lu, Chang-Qing Ke, Xiaobing Zhou, Manman Wang, Hui Lin, Deliang Chen & Houjun Jiang (2018) Monitoring land deformation in Changzhou city (China) with multi-band InSAR data sets from 2006 to 2012, International Journal of Remote Sensing, 39:4, 1151-1174, DOI: [10.1080/01431161.2017.1399474](https://doi.org/10.1080/01431161.2017.1399474)

To link to this article: <http://dx.doi.org/10.1080/01431161.2017.1399474>



Published online: 05 Nov 2017.



Submit your article to this journal [↗](#)



View related articles [↗](#)



View Crossmark data [↗](#)



## Monitoring land deformation in Changzhou city (China) with multi-band InSAR data sets from 2006 to 2012

Yanyan Lu<sup>a</sup>, Chang-Qing Ke<sup>a</sup>, Xiaobing Zhou<sup>b</sup>, Manman Wang<sup>a</sup>, Hui Lin<sup>a</sup>,  
Deliang Chen<sup>c</sup> and Houjun Jiang<sup>c</sup>

<sup>a</sup>Jiangsu Provincial Key Laboratory of Geographic Information Science and Technology, Key Laboratory for Satellite Mapping Technology and Applications of State Administration of Surveying, Mapping and Geoinformation of China, Nanjing University, Nanjing, China; <sup>b</sup>Department of Geophysical Engineering, Montana Tech of The University of Montana, Butte, MT, USA; <sup>c</sup>College of Geographic and Biologic Information, Nanjing University of Posts and Telecommunications, Nanjing, China

### ABSTRACT

Over exploitation of groundwater in Changzhou city, China can cause land deformation, which in turn proves detrimental to the urban infrastructure. In this study, multi-band synthetic aperture radar (SAR) data sets (C-band Envisat ASAR, L-band ALOS PALSAR, and X-band COSMO-SkyMed) acquired from 2006 to 2012 were analysed using the synthetic aperture radar (SAR) interferometry (InSAR) time-series method to investigate the relationship between spatial-temporal distribution of land deformation and groundwater exploitation. Annual deformation rate inferred from multi-band interferograms ranges from  $-58$  to  $24$  mm year<sup>-1</sup>. Levelling-survey data were used to validate the multi-band InSAR measurements. The results showed that these two types of measurements were generally in agreement. Correlating groundwater-table and multi-band InSAR measurements at six groundwater-well stations showed that with the rise of the water table, the land rebounded. But in some areas with larger subsidence, continual subsidence was observed even though the water table rose after the prohibition of groundwater exploitation. This may have been caused by the hysteresis effect due to the consolidation of strata (especially for the creep deformation). Our study provides scientific evidence on the management of groundwater extraction and the assessment of land-subsidence hazards.

### ARTICLE HISTORY

Received 21 March 2017  
Accepted 17 October 2017

## 1. Introduction

Land deformation has been one of the most dramatic consequences of rapid urbanization around the world, especially in China where many cities have emerged and developed rapidly in recent decades (Baek et al. 2008; Qin and Perissin 2015; Yin, Yu, and Wilby 2016; Zhang et al. 2011; Perissin and Wang 2011). Some of the major damages to urban infrastructure such as highways, bridges, buildings, pipelines, and metros have been attributed to land deformation (Dong et al. 2014; Ma et al. 2011; Brunori et al. 2015;

**CONTACT** Yanyan Lu  [cdlyy52@163.com](mailto:cdlyy52@163.com)  Jiangsu Provincial Key Laboratory of Geographic Information Science and Technology, Key Laboratory for Satellite Mapping Technology and Applications of State Administration of Surveying, Mapping and Geoinformation of China, Nanjing University, Nanjing 210023, China

© 2017 Informa UK Limited, trading as Taylor & Francis Group

Hallegatte et al. 2013). In coastal cities, land subsidence increases the risks of flooding and seawater intrusion (Hallegatte et al. 2013; Abidin et al. 2013).

Changzhou, a medium-sized city in China, is a typical city with a significant land-subsidence problem due to overexploitation of groundwater during rapid urbanization. Land subsidence in this area was first reported in the early 1960s (Xue et al. 2008; Shi et al. 2012). In the 1970s, this area suffered seriously from the surface deformation (Wang et al. 2009). In the 1980s, this city experienced a maximum land subsidence of  $147 \text{ mm year}^{-1}$  (Wang et al. 2009). A survey report showed that the cumulative subsidence area of this region exceeded  $200 \text{ km}^2$  and that the average annual subsidence from 1979 to 1983 was about  $59.63 \text{ mm}$  (Hu 2011). In the 1990s, the subsidence rate in this city reached as high as  $109 \text{ mm year}^{-1}$  (Zhang et al. 2010).

To control the land subsidence and promote healthy urbanization, strategic measures such as the prohibition of groundwater exploitation within the urban city were implemented by the local government authorities of Changzhou city (Xie, Cao, and Xu 2009). Ground-based deformation-monitoring stations (e.g. global positioning systems [GPS], levelling) were installed by the city government to monitor and measure the surface deformation in 1983. At the beginning of the twenty-first century, the Chinese Geological Survey deployed the 'Investigation and monitoring of ground settlement in the Yangtze river delta area' project, in which temporal variations of land deformation in Changzhou were monitored by the GPS, precise levelling surveys, and water-table gauging in wells (Hu 2011; Zhu and Liu 2007).

Although highly useful land-deformation data were provided by these conventional ground-based monitoring methods deployed in multiple isolated locations, they could not provide extensive spatial details and comprehensive information about land deformation due to their low spatial resolution and limited areal coverage. To promote more sustainable urbanization and to monitor the spatial and temporal evolution of the deformation after the implementation of development policies, satellite synthetic aperture radar (SAR) interferometry (InSAR) technology was used.

InSAR has proved to be an invaluable remote-sensing technique for land-deformation measurements over large areas due to its ability to obtain imagery that has (since the 1960s) high-spatial resolution and sub-centimetre accuracies (Bürgmann, Rosen, and Fielding 2000). The differential interferometry technique used for calculating surface-deformation rates along the sensor line of sight (LOS) from imagery of a particular area is called differential InSAR (D-InSAR). The D-InSAR method has demonstrated its potential capabilities in high-accuracy surface-deformation monitoring of earthquakes (Wang et al. 2004), volcanic activity (Tomiyama, Koike, and Omura 2004), glacial movements (Hu et al. 2014), mineral-resource exploitation (Li et al. 2015), land subsidence (Akcin et al. 2010; Bayuaji, Sumantyo, and Kuze 2010), and landslides (Wang et al. 2013; Liao et al. 2012). However, spatial and temporal decorrelation severely restricted the use of D-InSAR, especially for the long-term time-series monitoring of urban areas. To overcome this limitation, advanced InSAR time-series-analysis methods, such as small baseline subset InSAR (SBAS-InSAR) and persistent scatterers InSAR (PS-InSAR), have been proposed to measure more accurately the long time-series surface deformation (Ferretti, Prati, and Rocca 2001; Ferretti, Prati, and Rocca 2000; Ferretti et al. 2007; Kampes 2006; Hooper 2006; Ferretti et al. 2011). The PS-InSAR method is suitable for monitoring precisely the

surface deformation through tracking the individual point-like targets placed on buildings, bare rocks, or other corner reflectors. The SBAS-InSAR method investigates the surface deformation over distributed scatterers (DS). A network of interferograms based on spatial–temporal baseline values below a threshold mitigates the decorrelation phenomena. The scientific literature has reported many successful case studies dealing with the detection and monitoring of surface deformation with the InSAR time-series method. Tung and Hu (2012) used the InSAR time-series method to infer land subsidence in Yunlin County using the C-band Envisat ASAR data acquired from 1996 to 1999. Considering that C-band exhibits a strong temporal decorrelation in vegetated areas, some researchers combined the L-band ALOS PALSAR data with the C-band Envisat ASAR data to study the relationship between groundwater and land subsidence (Kim et al. 2015; Kim et al. 2008). To obtain more complete and detailed deformation data of an affected area, Qu et al. (2014) used the InSAR time-series method to process multi-band (including C-, L-, and X-band) SAR data and found that subsidence-triggered fissures can cause localized surface displacement.

In this study, we use the SBAS-InSAR technology and multi-sensor InSAR data sets to investigate the spatial and temporal distribution of surface deformation in Changzhou city. The capabilities of the InSAR-based remote-sensing techniques as tools to monitor surface deformation are verified. First, the C-, L-, and X-band data sets acquired from the Envisat ASAR (with a data volume of 31 images), ALOS PALSAR (15 images), and COSMO-SkyMed (12 images), respectively, were processed to map the land deformation in Changzhou from 2006 to 2012. The distribution of deformation rates derived from the C-band Envisat and L-band ALOS images were compared. Second, precise levelling measurements were used to assess the accuracy of the InSAR measurements. Finally, the correlation between the InSAR time-series measurements and the water-table variations was analysed and the interaction between land subsidence and groundwater extraction was discussed.

## 2. Study area

Changzhou is located in the southern part of Jiangsu Province, China (Figure 1(a)). The ground elevation ranges from 3 to 10 m, and the elevation of mountains in this region ranges from 200 to 500 m. It is adjacent to the Yangtze River on the north and the Tai Lake on the south. The total area of Changzhou is approximately 4385 km<sup>2</sup>, and it measures approximately 98 km in the east–west direction and about 105 km in the north–south direction (Figure 1(a,b)). The main area of Changzhou city consists of four districts: Xinbei, Tianning, Zhonglou, and Wujin. This city has suffered from seawater intrusion since the middle Pleistocene, and a set of Quaternary deposits of clay, silty clay, silt, sand, and gravels therefor settled down. The thickness of the Quaternary strata distributed in Changzhou city ranges from 120 to 260 m. Figure 1(c) shows a geological cross section in Changzhou city along a profile as indicated by the northwest–southeast-oriented line segment in Figure 1(b). The Quaternary deposits in the study area are composed of four aquifers: one unconfined aquifer and three confined aquifers that are denoted as UA, A1, A2, and A3, respectively, from the top to the bottom in Figure 1(c). Conventionally, groundwater with 50 m deep is shallow (such as UA and A1) otherwise is deep

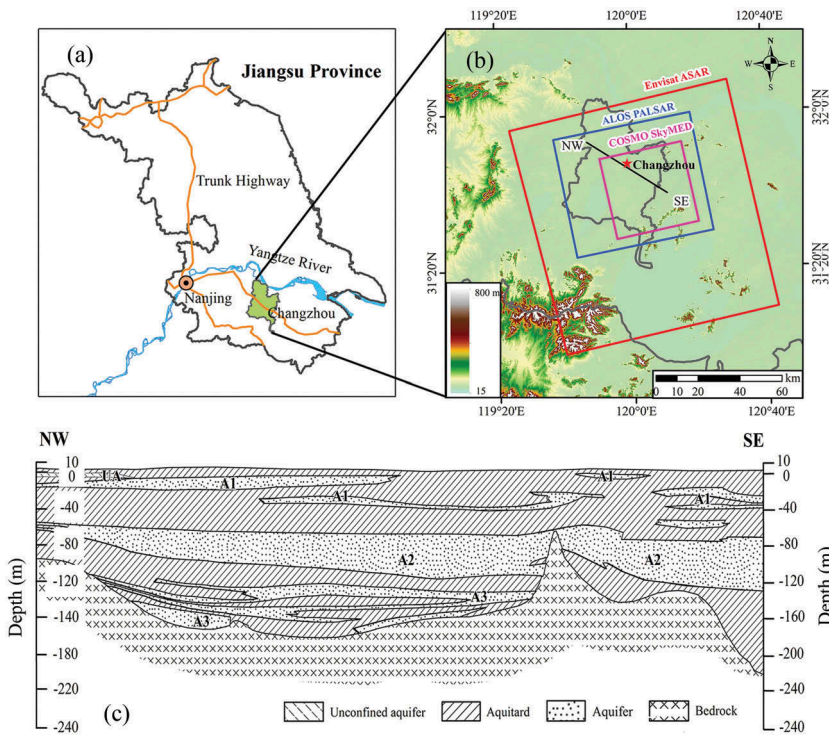


**Figure 1.** (a) Geographical location of Changzhou city, China. The green region enclosed by the grey polygon in (a) represents the study area. (b) The shaded relief map derived from the SRTM DEM. The coverage of the Envisat ASAR, ALOS PALSAR, and COSMO-SkyMed image data are indicated by the red, blue, and purple rectangular box, respectively. The northwest–southeast-oriented line segment indicates the location of the geological cross section of Changzhou city shown in (c).

(such as A2 and A3). The A2 aquifer is a compression stratum and it was the main exploited aquifer (Miao et al. 2007; Wang et al. 2009). This aquifer is almost continuous along the northwest–southeast direction with a thickness of 10–50 m (Figure 1(c)). The depth of the top of A2 increases from 50 m in northwest to 130 m in southeast. Groundwater overexploitation in A2 is believed to be the main cause for the land subsidence in Changzhou city.

As one of the most economically developed cities in the Yangtze River Delta region, Changzhou city has urbanized rapidly. According to a report from the Statistics Bureau of Jiangsu Province, the urbanization rate of Changzhou had reached 68.70% by the end of 2014, while the population increased from 3.41 million in 2002 to 4.69 million in 2014. The rapid urbanization and increased population led to a significant increase in the demand for resources such as groundwater and land for industrial and residential purposes. Excessive extraction of groundwater and continually increasing surface loading caused by buildings finally resulted in ground subsidence hazards in this area. Along with the subsidence hazards are ground cracks, damage to urban infrastructure, and increased threat of flood disasters. Thus, it becomes particularly urgent to investigate the surface deformation in Changzhou city and to provide more scientific data in promoting the sustainable urban development of this area.

### 3. Data sets

In order to explore the land subsidence in Changzhou city, multisource data were used. The multi-band SAR data were used to detect the distribution and settlement of the deformation area. Levelling data were essential to verify the accuracy of the InSAR measurements. Groundwater data were used to analyse the cause of land deformation.

#### 3.1. SAR data

Compared to the shorter wavelengths of infrared and visible EM radiation, SAR microwaves have longer wavelengths that allow them to penetrate fog and clouds. This unique property allows SAR to provide imagery with less interference from the weather than the infrared and visible EM radiation. The high temporal sampling rate and spatial resolution of SAR data allows SAR to provide risk analysis of urban cities and fulfils the requirement of high-precision surface-deformation monitoring of large areas for extended time periods. With the development of SAR sensors, more SAR data can be acquired to study urban deformation.

The quality of SAR image is closely related to the wavelength of Radar. In the vegetated region, the vegetation will scatter and attenuate the radar signal, which makes the echo signal weaker and finally impairs the quality of the image SAR image. This extent of the effects caused by vegetation is different depending on the wavelength of Radar: long wavelength bands are less affected by vegetation than short wavelength bands. The wavelength of L-band is about 23.6 cm, far greater than the C-band (5.6 cm) and X-band (3.1 cm), so the penetrability of L-band is higher than the C-band and X-band. The strong penetrability of L-band makes a lot of radar wave penetrating the canopy and arrives at the trunk or directly penetrating vegetation and reach the ground. In the subsequent echo stage, the attenuation of the echo signal is relatively weak compared to the C- and X-band. Scattering of radar signals in the vegetation will cause decorrelation of radar signal, reducing the quality of radar interferograms. The above features ultimately led to higher quality of SAR image of the L-band than the C- and X-band in the vegetated area. In this study, to better describe the land-deformation characteristics with less influence from vegetation of Changzhou, three types of SAR data were used (see Table 1): 31 Envisat ASAR images in the C-band, 15 ALOS PALSAR images in the L-band, and 12 COSMO-SkyMed images in the X-band. These SAR images cover the period from 2006 to 2012: April 2006–April 2010 for Envisat ASAR, January 2009–March 2011 for ALOS PALSAR, and July 2011–July 2012 for COSMO-SkyMed. Meanwhile, the X-band COSMO-SkyMed, with higher ground resolution than both ASAR and PALSAR, can provide more detailed information about land deformation. Therefore, the synthesized

**Table 1.** C-band, L-, and X-band SAR data information used in this study.

Sensor	Envisat ASAR	ALOS PALSAR	COSMO-SkyMed
Band	C	L	X
Wavelength (cm)	5.6	23.6	3.1
Heading (°)	-11.9326555	-10.2740400	169.1276146
Incidence angle (°)	22.7998	38.7236	29.4297
Polarization	VV	HH, HV	HH
Orbit type	Ascending	Ascending	Ascending
Spatial resolution (m)	30	10	3
Number of images	26	15	12
Data range	20 April 2006–29 April 2010	17 January 2009–10 March 2011	21 July 2011–14 July 2012

application of these three bands of SAR data allows us to analyse the observed surface deformation comprehensively. To remove the topographic phase from the interferograms, a Shuttle Radar Topography Mission (SRTM) DEM with a 3 as (90 m) resolution was used. The precise orbital data provided by the Technical University of Delft were used for processing the orbit corrections on Envisat ASAR data (Scharroo and Visser 1998).

### 3.2. Levelling data

To understand the status of the land deformation in Changzhou, the government has carried out levelling measurements for many years (Li and Wu 2015; Wu et al. 2014). In this study, the levelling data from 11 levelling monitoring sites acquired from 2006 to 2014 provided by the Changzhou Surveying and Mapping Institute were used to validate the accuracy of the InSAR measurements (Figure 2(a)). These levelling data were obtained from levelling method. Generally speaking, the levelling method is a method that measuring the vertical distance directly. This method is used to determine differences in elevation between points that are remote from each other by using a surveyor's level together with a graduated measuring (Yin 2013). The distribution and the annual variation of the levelling data indicated that the subsidence areas concentrate in the Wujin District (Figure 2(b)).

### 3.3. Groundwater data

In Changzhou, the main layer from which groundwater is extracted is the second confined aquifer (A2, Figure 1(c)). To explore the relationship between the variation of the water-table and the land deformation, groundwater-table data of the second confined aquifer, obtained from six water wells (labelled as W1–W6 in Figure 2(a)), were used in this study. These data were provided by the Jiangsu Province Hydrology and Water Resources

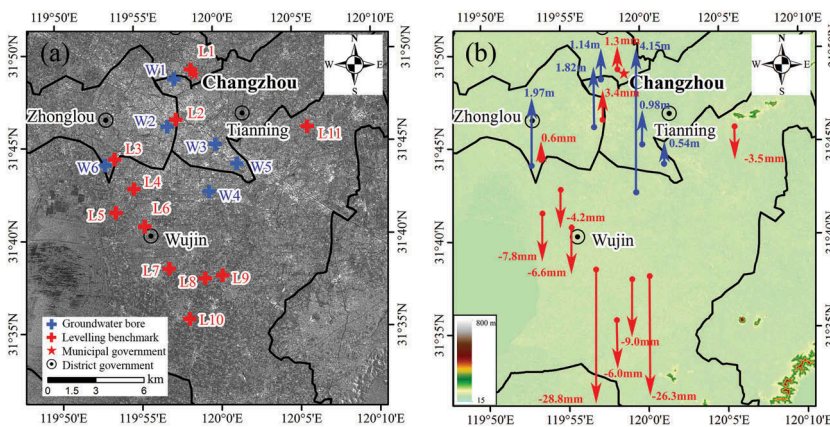


**Figure 2.** (a) The location map of the groundwater wells and levelling benchmarks distributed in the study area. The cross sign in blue represents groundwater wells and the cross sign in red represents the levelling benchmarks. (b) The mean annual measurements at the groundwater wells and levelling benchmarks showed in (a). The arrows in red and blue represent levelling and groundwater sites, respectively, and the length of arrows indicates the amount of changes.

Investigation Bureau. From the distribution and the annual variation of groundwater, we found that the groundwater in Changzhou city is in rebound stage (Figure 2(b)).

## 4. Processing methods

SBAS-InSAR is an InSAR-based technique, which has proved to be effective in monitoring land deformation (Berardino et al. 2002, 2001; Lanari et al. 2004, 2007). In this study, the SBAS method was used to investigate the land deformation in Changzhou city.

### 4.1. SBAS method

Time series of land deformation was obtained from the SBAS-InSAR method. The method was first proposed by Berardino and Lanari (Berardino et al. 2002, 2001; Lanari et al. 2004, 2007). This method divided the whole SAR data set available into different subsets. Interference pairs were made by multiplying a master complex image with a conjugate of a slave complex SAR image in every subset according to the following principle: within each subset, the spatial–temporal baseline was smaller than a threshold defined by the user, but between subsets, the baseline was relatively larger. The purpose of such an approach was to mitigate both spatial and temporal decorrelations and to preserve high interferometric coherence. The SBAS-InSAR method could identify DS that were surrounded by completely decorrelated targets. Then, the observed phase shift resulting from the DS can be expressed as in the following equation.

$$\varphi_{\text{int},i}^n = \varphi_{\text{def},i}^n + \varphi_{\text{top},i}^n + \varphi_{\text{atm},i}^n + \varphi_{\text{noise},i}^n \quad (1)$$

The right side of the equation represents the component phase of the  $i$ th pixel in the  $n$ th differential interferogram  $\varphi_{\text{int},i}^n$ .  $\varphi_{\text{def},i}^n$  is the deformation phase caused by the movement of a pixel along the satellite LOS direction;  $\varphi_{\text{top},i}^n$  is the residual topographic phase caused by errors in the DEM;  $\varphi_{\text{atm},i}^n$  is the atmosphere phase caused by the atmospheric delay between SAR data acquisition times;  $\varphi_{\text{noise},i}^n$  is the noise phase caused by multiple factors such as registration errors, thermal noise, etc. By modelling, retrieving, and hence removing the phase  $\varphi_{\text{top},i}^n$ ,  $\varphi_{\text{atm},i}^n$ , and  $\varphi_{\text{noise},i}^n$ , a very accurate measure of surface deformation  $\varphi_{\text{def},i}^n$  can be achieved.

### 4.2. Data processing

In the SBAS-InSAR approach, thresholds of spatial–temporal baseline and Doppler centroid difference were applied to generate interferograms with SAR image pairs that maximize the InSAR coherence. In this study, we only considered the spatial–temporal baseline since the Doppler centroid difference was negligible. We set the spatial baseline to be smaller than 380, 1800, and 800 m and with the temporal interval smaller than 400, 360, and 180 days for images in the C-, L-, and X-bands, respectively. Under such a design, 123 interferograms in the C-band (Figure 3(a)), 62 interferograms in the L-band (Figure 3(b)), and 42 interferograms in the X-band were generated (Figure 3(c)). The topographic and reference phases in the interferograms were removed by using the 3 as SRTM DEM data. The precise orbit

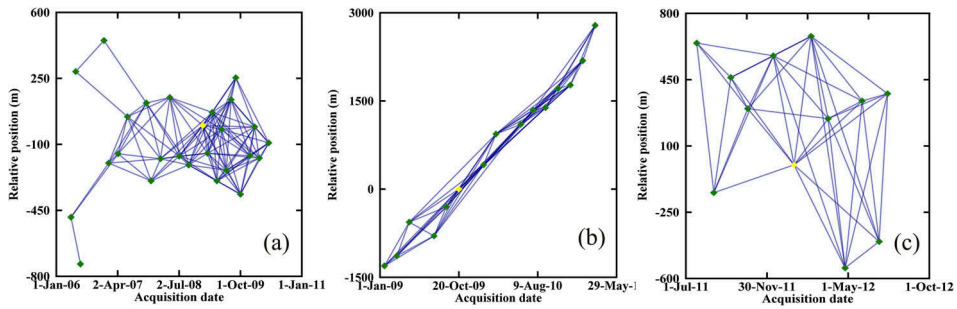


**Figure 3.** The baselines for all of the InSAR image pairs. Panels (a–c) show the relationship between the temporal and perpendicular baselines of the C-band Envisat ASAR image pairs, L-band ALOS PALSAR image pairs, and the X-band COSMO-SkyMed image pairs, respectively.

information provided by Delft Institute for Earth-Oriented Space Research was used to remove the orbit error in the Envisat ASAR C-band radar data. Adaptive spectral filtering was used to reduce the interferometric noise from the interferograms. The minimum cost flow algorithm was used for phase unwrapping (Costantini 1998). After the above steps were completed, we discarded the interferograms with false-phase unwrapping and low coherence. To ensure the InSAR measurement accuracy, amplitude-dispersion-index thresholding and correlation-coefficient thresholding were used. After the above-mentioned processing steps, least squares and singular-value decomposition methods were used to calculate the land deformation in a long time series.

In addition, the atmospheric phase cannot be ignored during the SBAS-InSAR processing as it can significantly affect the accuracy of the measurement. A spatial low-pass filtering followed by a temporal high-pass filtering was used to remove atmospheric artefacts. Also, noise phase was removed during this processing. Afterwards, we obtained the time-series surface-deformation measurements at each DS location.

While integrating the C-, L-, and X-band InSAR data, a problem occurred: there were some data gaps among these three groups of InSAR pairs (Figure 3). These gaps caused the difficulty in analysing the InSAR results. We use the following steps to fill the data gaps: first, we projected the three InSAR deformation results (C-, L-, and X-band) onto the vertical direction to ensure the consistency of the results, as the three InSAR measurements were along different LOS directions; second, the linear interpolation method was adopted to calculate the deformation value  $y_0$  on 17 January 2009 from the Envisat ASAR values; third, we set the first deformation values of ALOS PALSAR (17 January 2009) from  $x_0$  to  $y_0$  and the other deformation values of ALOS plus the difference  $y_0 - x_0$ , then the gap between Envisat and ALOS was filled. The method described above was also used to fill the gap between the last ALOS PALSAR data acquisition (10 March 2011) and the first COSMO-SkyMed data acquisition (21 July 2011). The integrated results can provide more complete and detailed information about the land subsidence measured from different bands. As the C-band and X-band are sensitive to small-scale deformation, while the L-band is sensitive to large-gradient deformation, the integration of the Envisat ASAR, ALOS PALSAR, and COSMO-SkyMed data was considered more robust than results obtained from single-SAR data sources (Jiang et al. 2011).

## 5. Results

### 5.1. Comparison of deformation results derived from C-, L-, and X-band data

In this section, we analysed and compared the Envisat ASAR, ALOS PALSAR, and COSMO-SkyMed InSAR time-series measurements. In order to make the comparative results reliable, we projected the deformation values from the LOS direction to the vertical direction.

After processing the SAR data in the C-, L-, and X-bands with the SBAS-InSAR method, three deformation-rate maps along the vertical direction over the study area were generated. An obvious land subsidence region in the Wujin district was observed from the deformation images of the three bands (Figure 4). It can be seen that although the time spans of the three bands SAR data were different, the surface deformation trends were consistent (Figure 4). The number of DS in the L-band (about 2566,411) was larger than those observed in either the C-band (about 1658,358) or the X-band (about 1900,436), especially in the vegetated areas. This was because the L-band microwave radiation, having a longer wavelength (about 23.6 cm), could get better return signals from the ground than the C-band (about 5.6 cm) and the X-band (about 3.1 cm) radiation in uneven terrains and vegetated areas.

Some regions with obvious land subsidence can be observed from the three deformation-rate maps (Figure 4). The deformation magnitude of the three SAR results was similar, ranging from  $-58$  to  $24$   $\text{mm year}^{-1}$ . However, the deformation rate along profile PP' in Figure 4 presented a subtle difference among the C-, L-, and X-band InSAR results: an extended subsided area appears in the northeast part of Changzhou in the L-band SAR result, but this extension was absent in the C-band and X-band results. This difference might be due to the stronger penetrability of the L-band radiation in the vegetated regions and this characteristic enhanced the monitoring ability of the L-band radar in this area compared to the C- and X-band radars. Figure 5 shows the deformation rate along the profile PP' in Figure 4. It was found that the distribution of the land-subsidence rate along PP' was similar

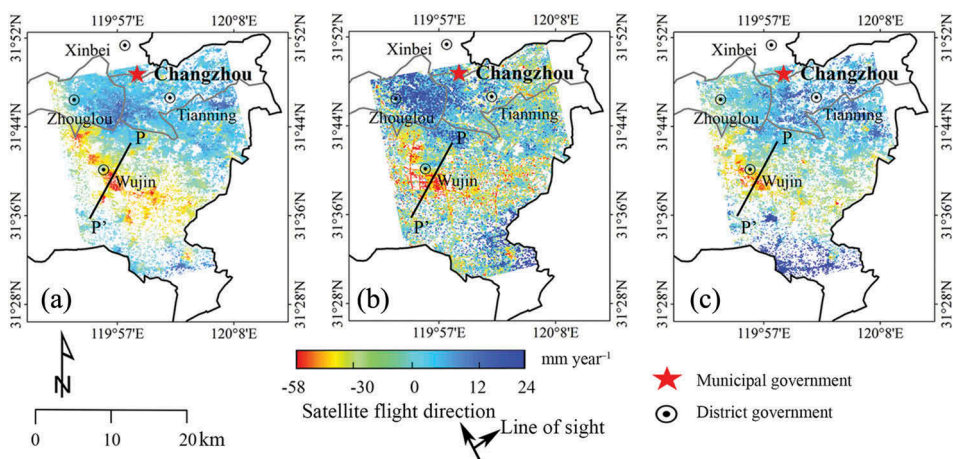


**Figure 4.** Deformation rates projected onto the vertical direction for the C-, L-, and X-bands at the selected study area. The PP' is the location of the profile along which the deformation rate will be shown in Figure 5. (a) Envisat ASAR measurements, (b) ALOS PALSAR measurements, and (c) COSMO-SkyMed measurements.

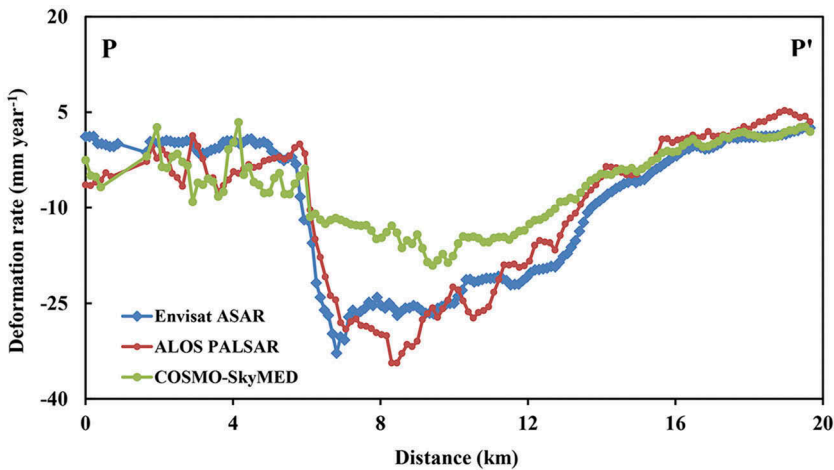


**Figure 5.** Deformation rate along the profile PP' in Figure 4.

among the three kinds of SAR data. In the subsidence funnel centre, the X-band (the centre subsidence was  $-18.6 \text{ mm year}^{-1}$ ) detected smaller deformation magnitudes than the C-band (the centre subsidence was  $-32.8 \text{ mm year}^{-1}$ ) and the L-band (the centre subsidence was  $-34.3 \text{ mm year}^{-1}$ ). This difference may be caused by the following factors: (1) small data set (12 SAR data) and short time span (only 1 year from 2011 to 2012) of the X-band SAR data, (2) the lesser penetrating capacity of the X-band than the C- and L-band, and (3) the gradual decrease of groundwater exploitation after the implementation of a strict groundwater exploitation policy and the improvement of urban infrastructure after 2010 (Feng 2011; Editor Board of Changzhou 2009).

Through the comparison of the C-, L-, and X-band InSAR results, we conclude that the comprehensive joint use of multi-band SAR data can provide more complete and detailed information about surface deformation.

### 5.2. Deformation rate by integrating the C-, L-, and X-band SAR images

The results showed in Figure 4 indicate that the surface deformation in Changzhou was evident, primarily in the range of  $-54$ – $15 \text{ mm year}^{-1}$  obtained from the Envisat ASAR data of the C-band (from April 2006 to April 2010),  $-58$ – $20 \text{ mm year}^{-1}$  obtained from the ALOS PALSAR data of the L-band (from January 2009 to March 2011), and  $-49$ – $24 \text{ mm year}^{-1}$  obtained from the COSMO-SkyMed data of the X-band (from July 2011 to July 2012). The subsided area in our study area decreased from 175 to 151  $\text{km}^2$  in 7 years (e.g. from 2006 to 2012). This change may be attributed to the subsidence control measure taken by the government of Changzhou city to limit groundwater extraction (Xie, Cao, and Xu 2009).

It is worth noting that although the time spans of the Envisat ASAR and ALOS PALSAR data sets have overlapping period of about 16 months, the deformation pattern was not completely consistent. Therefore, to find out the difference between the two kinds of SAR data in measuring land deformation, correlation analysis was performed and the results are shown in Figure 6. As the spatial distributions of the DS points did not completely coincide in these two measurements, we used the nearest-neighbour

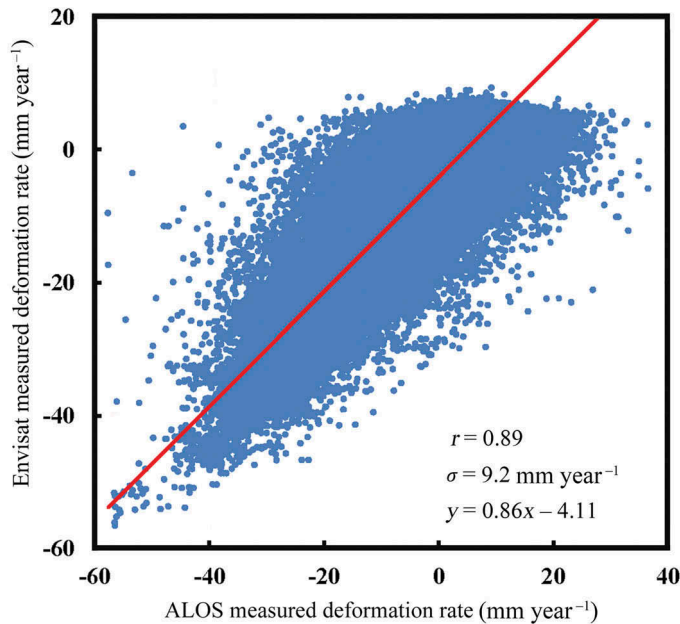


**Figure 6.** The distribution of DS obtained from the ALOS PALSAR and Envisat ASAR images for the common monitoring period spanning from January 2009 to April 2010.

interpolation to make the comparison result reliable. The correlation coefficient  $r$  is used to study the relationship between two data sets and is defined as follows,

$$r = \frac{\text{Cov}(x, y)}{\sigma_x \sigma_y} \quad (2)$$

where  $\text{Cov}(x, y)$  is the covariance of  $x$  and  $y$ ,  $\sigma_x$  and  $\sigma_y$  are the standard deviations of  $x$  and  $y$ , respectively. This correlation coefficient is also used in Sections 6.1 and 6.2.

A correlation coefficient ( $r$ ) of 0.89 between the two data sets suggested that the deformation rate in Changzhou, derived from the two different data sets, was well correlated. The standard deviation of the deformation-rate difference was  $9.2 \text{ mm year}^{-1}$ . The difference in magnitude between the two data sets may have been caused by the following three factors: (1) data from different satellites and sensors may have different measurement precisions including orbit accuracy, (2) the two data sets were not acquired at exactly the same times, (3) some errors in SBAS processing, and (4) the L-band SAR data have a higher accuracy than the C-band data in monitoring land subsidence (Ge et al. 2014) (Envisat ASAR data in the C-band and ALOS PALSAR data in the L-band).

The annual average deformation-rate maps (Figure 7) derived from the Envisat ASAR, ALOS PALSAR, and COSMO-SkyMed data showed that the Wujin District suffered the most serious land subsidence and the maximum subsidence rate in this district reached  $-58 \text{ mm year}^{-1}$ . There were no obvious surface subsidence patterns in the Zhonglou, Tianning, and Xinbei districts. Several researchers have suggested that the land subsidence in some areas in Changzhou city could have been caused by two important factors during urbanization: overexploitation of groundwater and soil consolidation (Miao et al. 2007; Zhang et al. 2007;

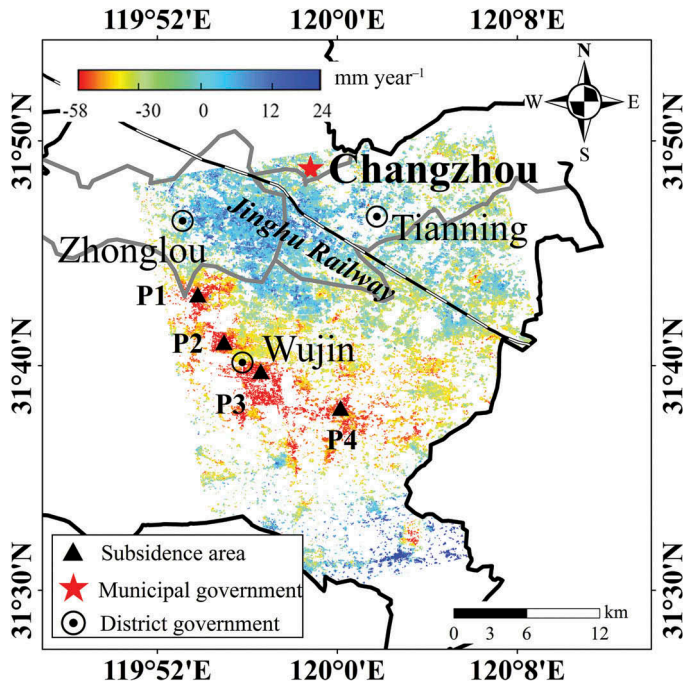


**Figure 7.** The distribution of deformation rate in Changzhou city, calculated from the Envisat ASAR, ALOS PALSAR, and COSMO-SkyMed SAR data. The black triangles marked with P1, P2, P3, and P4 represent the points located in the rapidly subsiding areas. The displacement rate along the Jing-Hu Railway is shown in Figure 8.

Shi et al. 2008; Xu et al. 2012). Figure 8(a) shows the severe subsidence areas over the Google Maps, where artificial structures with white, brown, or blue roofs were within the industrial zones and red were in the residential zones. It indicated that areas with significant subsidence mostly happened in the industrial zones, where groundwater resources were possibly over-exploited for industrial production. We also discovered that the maximum annual deformation rate of subsidence bowls marked as P1–P4 in Figure 8(a) was  $-38.92$ ,  $-32.54$ ,  $-41.26$ , and  $-31.25$   $\text{mm year}^{-1}$  (Figure 8(b)), respectively. The variation trends at the four points may suggest that the subsidence in these areas may continue for a while. An investigation of land subsidence in Changzhou city by Hu (2011) indicated that the over exploitation of groundwater for industrial purposes was the main cause of land subsidence. This suggested that the main cause of land subsidence distributed in Figure 8(b) might be the over-extraction of groundwater for industrial production. As the subsidence areas were found near or at the industrial and residential areas where the increased urban and industrial development were also found (Figure 9), it is likely that construction of infrastructures such as residential, industrial, and commercial buildings increased the surface load, leading to soil consolidation and contributing to land subsidence. This urban development and the concurrent land surface subsidence may indicate that the urban development may contribute to the subsidence, but its quantitative contribution may need further investigation. The other deformation area was discovered in the eastern part of Changzhou city where Jing-Hu (JH) Railway, an important transport route, also passes through this area (Figure 7). Figure 10 shows the vertical deformation rate of the JH Railway. The mean vertical deformation swath profile

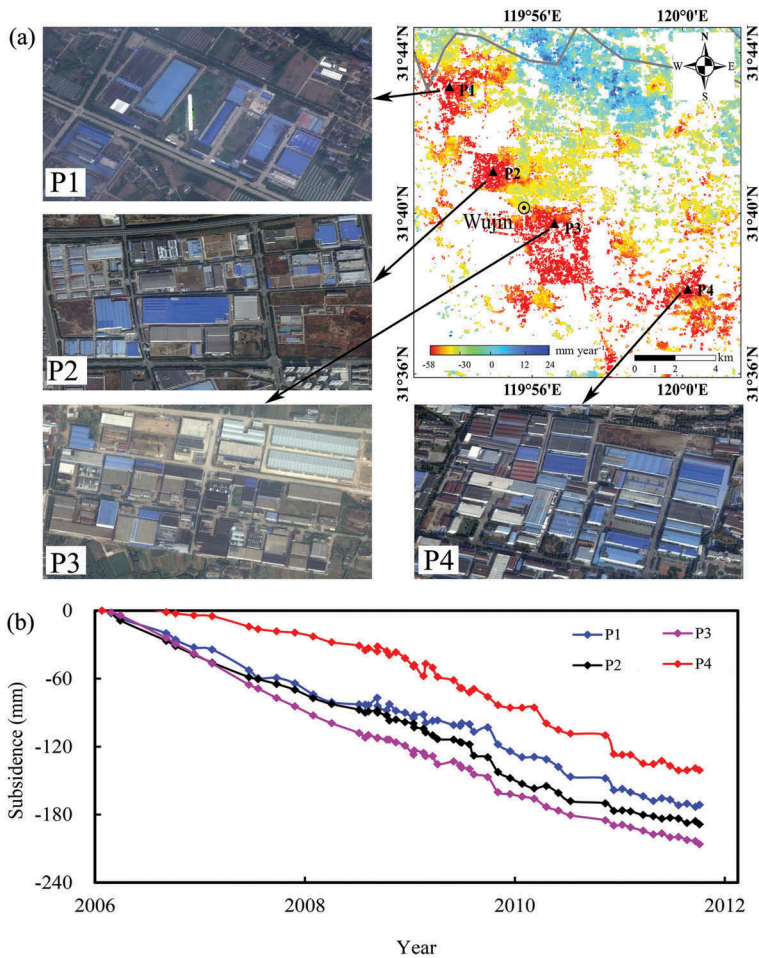


**Figure 8.** (a) The map of subsidence rate for the four regions labelled as P1, P2, P3, and P4. Insets are optical satellite images (©Google Image) showing the buildings at these four sites. (b) Land subsidence derived from the multi-band SAR data sets at sites P1–P4.

along the JH Railway (Figure 10(a)) indicates that the deformation along this railway is relatively small, except at the Niutang Industrial Park (ranges from  $-28$  to  $-12$   $\text{mm year}^{-1}$ ). Figure 10 also shows that the deformation rate of the Changzhou Railway Station is small (ranges from  $-3$  to  $10$   $\text{mm year}^{-1}$ ). The subsidence of the JH Railway at the Niutang section might be caused by the excessive groundwater extraction and soil consolidation due to surface loading.

## 6. Discussion

### 6.1. Comparison between the InSAR and levelling measurements

To assess the InSAR measurements, the InSAR-derived subsidence values were compared with levelling observations. To ensure the reliability of the comparison results, we projected the two deformation measurements (InSAR and levelling measurements) onto

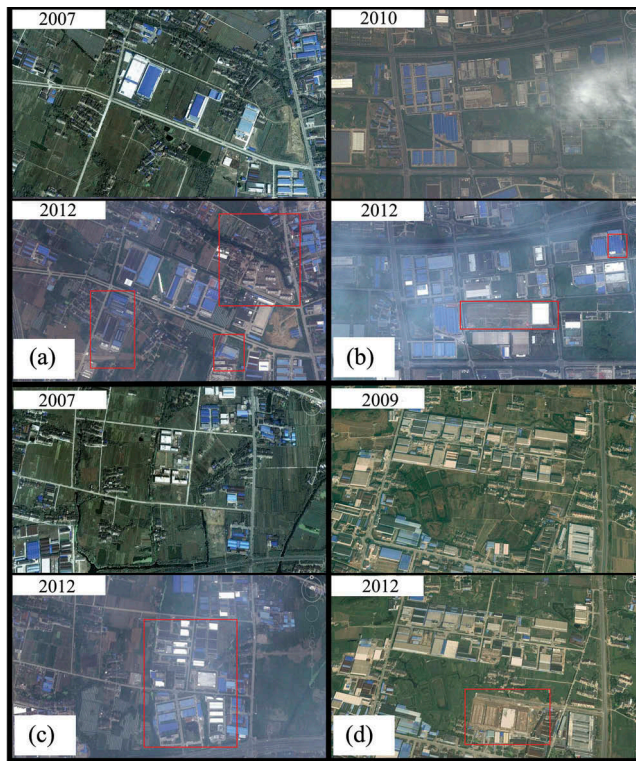


**Figure 9.** The expansion map of urban and industrial development in Google images. Figure parts (a–d) represent the expansion map of regions around sites P1, P2, P3, and P4 marked in Figure 8, respectively. The red squares represent the region of variation.

the vertical direction. Considering the centres of the corresponding InSAR pixels may not overlap exactly over the locations of the levelling benchmarks, arithmetic-mean method was used. First, we selected all the InSAR pixels whose centres were within 100 m of the benchmarks. Second, we calculated the average displacement values from the selected InSAR pixels. The calculated mean values were taken as the InSAR measurements at the positions of the levelling benchmarks. Finally, the InSAR and levelling measurements were compared. The comparison results between the InSAR and levelling measurements are shown in Figure 11 and Table 2. The InSAR and levelling observations agreed generally well, with a minimum and maximum difference of 0.2 and 5.1 mm year<sup>-1</sup>, respectively. The differences between the InSAR and levelling measurements were likely caused by the following factors: (1) the deformation rate obtained from the InSAR was the projection of the overall deformation along the SAR's LOS direction, while the levelling measurements were the projection along the vertical direction; (2) the InSAR measurements were the average of all pixels within the 100 m range around the benchmarks; (3) each InSAR measurement was the average of the whole pixel scale while each levelling measurement was at the point scale; and (4) the errors in the InSAR and levelling measurements themselves may be different. Figure 11 showed a good agreement between the two data sets with  $r = 0.97$ . The standard deviation of the deformation rate between the two data sets was 10.2 mm year<sup>-1</sup>. Table 2 was the

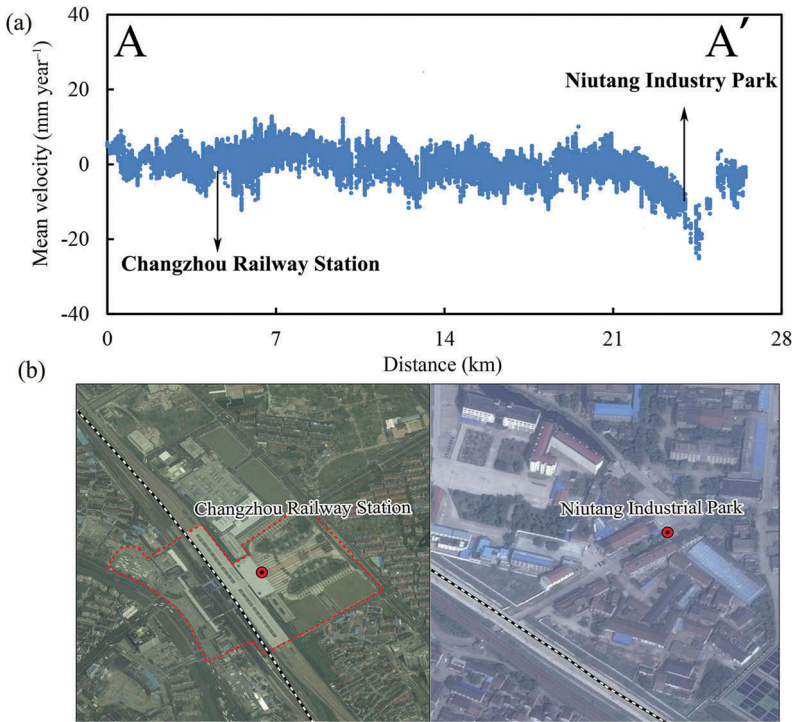


**Figure 10.** (a) Deformation rate along Jing-Hu Railway with buffer distance of 400 m to both sides of the line. (b) The spatial relationship among Jing-Hu Railway, Changzhou Railway Station and Niutang Industrial Park. The black and white line represent Jing-Hu Railway.

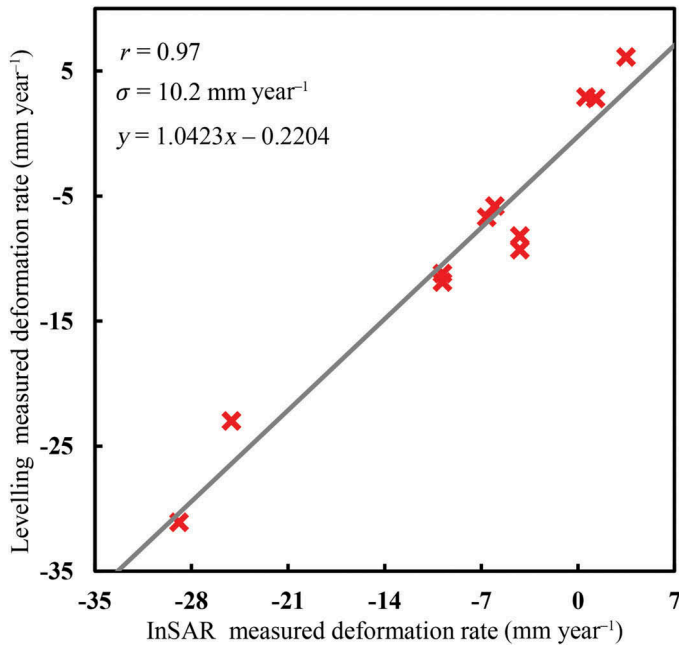


**Figure 11.** Comparison between the InSAR-derived and levelling-derived deformation rates at the levelling survey points showed in Figure 1.

**Table 2.** Settlement errors between the InSAR and levelling measurement at 11 levelling survey points marked in [Figure 2](#).

Levelling survey points	InSAR measurements (mm year <sup>-1</sup> )	Levelling measurements (mm year <sup>-1</sup> )	Error (mm year <sup>-1</sup> )
L1	2.7	1.3	1.4
L2	6.1	3.4	2.7
L3	2.9	0.6	2.3
L4	-7.2	-4.2	-3.0
L5	-10.2	-7.8	-2.4
L6	-6.7	-6.6	-0.1
L7	-30.1	-28.8	-1.3
L8	-10.9	-9.0	-1.9
L9	-23.7	-26.3	2.6
L10	-5.8	-6.0	0.2
L11	-7.2	-3.5	-3.7

subsidence error between the InSAR and levelling measurements at 11 levelling survey points. The difference between the InSAR and levelling measurements showed that the error values of L1–L10 were within  $\pm 3.0$  mm year<sup>-1</sup> and L11 was  $-3.7$  mm year<sup>-1</sup>. The high value of  $r$  and the small difference indicated that the InSAR time-series measurements agreed reasonably well with the ground truth in measuring the surface deformation. It indicated that the InSAR measurements are reliable in the monitoring of land deformation. The InSAR measurements, with higher temporal resolution than the levelling survey, are also able to provide more detailed information about surface deformation in Changzhou city. This information is very important for implementing surface subsidence control measurements and hydrogeological research. In summary, the combination of the InSAR and levelling measurements can provide better analysis of land deformation in both spatial and temporal domains.

## 6.2. Correlation between the land subsidence and groundwater

According to the historical survey data, the land subsidence in Changzhou city started in the 1960s (Hu et al. 2009; Shi et al. 2012). The subsidence reached  $-50.63$  mm year<sup>-1</sup> between 1979 and 1983, and the maximal subsidence reached  $-100$  mm (Wang et al. 2009). Since 1996, the city government started limiting groundwater withdrawal and land subsidence in Changzhou slowed down and the subsidence rate also decreased from  $-60$  mm (in 1994) to  $-10$  mm (in 2005). To understand the influence of groundwater-table variation on the ground surface deformation, the deformation values obtained from the InSAR measurements were regression analysed with the change of groundwater table at six water wells ([Figure 2](#)). The procedures discussed in [Section 6.1](#) were also used to match the InSAR pixels to the point of water wells.

[Figure 12](#) shows the comparison between the InSAR-derived and groundwater-table deformation rates and a negative  $r = -0.72$  was found. [Figure 13](#) showed the time series of the InSAR-measured deformation (displacement) and groundwater table in the second aquifer. Land surface rebound was found at the groundwater well stations W1, W2, W3, and W5 with the increase of groundwater table at these stations. To better identify the influence of groundwater change on the ground surface deformation, a correlation analysis between the values of groundwater-table and surface deformation was performed. Positive  $r$  of 0.91, 0.98,

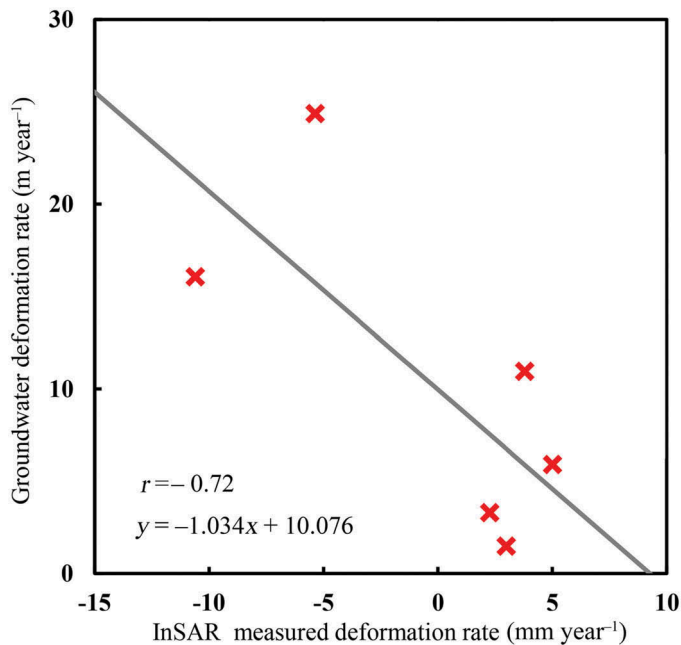


**Figure 12.** Comparison between the InSAR-derived and groundwater-table deformation rates at the groundwater survey stations showed in Figure 2(a).

and 0.94 were observed at well stations W1, W2, and W5, respectively; a lower  $r$  of 0.65 was observed at station W3 (see Figure 13). The lower  $r$  of W3 was caused by the decline of groundwater table during 2009–2010. On the whole, the land surface deformation agreed well with the changes in groundwater levels in these four groundwater stations. These groundwater stations were located in the main urban region, and the uplift of the land surface in this region was due to strict regulatory measures to prohibit the exploitation of groundwater (Xu et al. 2015). The relationship between InSAR measurements and groundwater level change also indicated that for every 1 m rebound in groundwater level, it would induce 2 mm land rebound in W1 and W2 and 5 mm rebound in W3 and W5. This difference was closely related to the effects of surface load. From the distribution of building around the four water wells, we found that high buildings were distributed around wells W1 and W2, but low buildings are distributed around wells W3 and W5 (Figure 14). According to the research by Meng (2011), the surface load around wells W1 and W2 will be greater than that at the wells W3 and W5. As the rebound of the land was affected by the surface load, it is thus expected that the rate of land rebound is greater at W3 and W5 than W1 and W2. It is also need to notice that the magnitude of land rebound is also influenced by other factors, such as the different geological structure, geotechnical property, and stratum thickness at the observed wells.

However, the land deformation was not always in synchronization with the groundwater-table change since 2006, especially at water wells W4 and W6, which were located in the Wujin District. Although the groundwater table rose, land subsidence was still observed at wells W4 and W6. As the InSAR and levelling measurements are well consistent with each other during this period, the measurements obtained were considered to be reliable. Negative  $r$  of  $-0.88$  and  $-0.98$  were found at wells W4 and W6, respectively (see Figure 13). The results

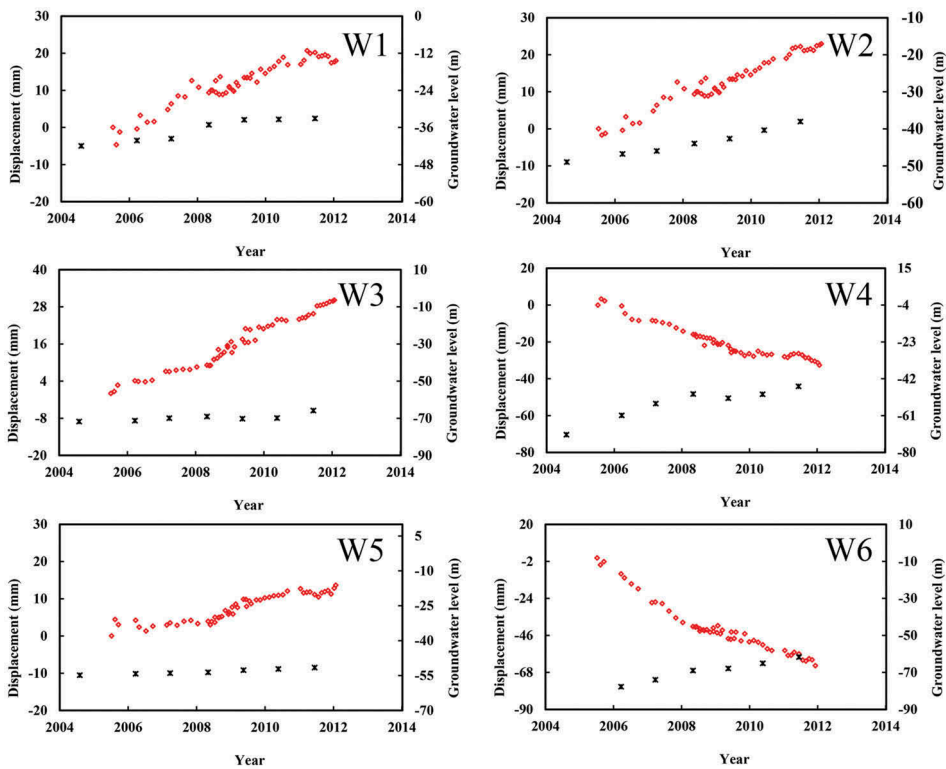


**Figure 13.** Groundwater-table level and land deformation from 2006 to 2012 at the groundwater wells in Changzhou. Stations W1–W6 are the water wells marked in Figure 2(a). The red diamond indicates InSAR measured displacement value and black cross indicates groundwater level value.

suggest that the change of groundwater table has mixed effects on the surface deformation during 2006 and 2012. According to relevant studies, the land subsidence in some area of Changzhou city has been effectively controlled and the land deformation showed an upward trend since 2004 (Hu 2011; Zhang et al. 2010). These areas include the Xinbei District, the eastern part of the Zhonglou District (where the well W2 is located), and the western part of the Tianning District (where the wells W1, W3, and W5 are located) (Hu 2011). The research by Xu, Zhou, and Gao (2011a, 2011b) indicated that the hysteresis phenomena exist in the consolidation of strata during the process of the groundwater-table variation and the state of consolidation of strata plays a very important role in the land subsidence. As the wells W4 and W6 are located in the settlement area from 2001 to 2004 (Hu 2011), it indicated that the consolidation of the strata around the wells W4 and W6 had not completed after the exploitation of underground water was prohibited. The strata in this area were still in a state of compression, resulting in the continual subsidence observed even the groundwater table rose (Zhang et al. 2010; Xu, Zhou, and Gao 2011a; Xu, Zhou, and Gao 2011b). This process will continue until the consolidation of the strata is completed. It is also worth noting that the second confined aquifer in Changzhou consists of clay, fine sand, and medium-coarse sand with gravel. Creep deformation played an important role during the consolidation of the strata, especially at the stage of groundwater recovery under this geological condition. This effect caused hysteresis of the deformation even though the groundwater table rose (Shi et al.

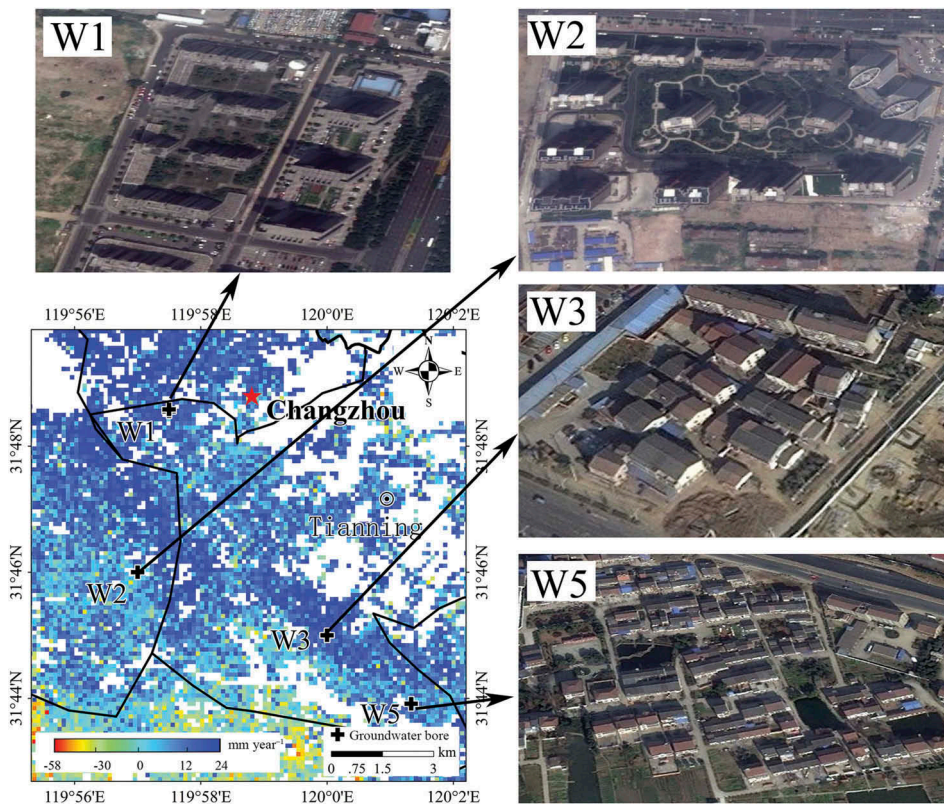


**Figure 14.** Map of the distribution of water wells and buildings in Google Maps. The groundwater wells W1, W2, W3, and W5 are marked in Figure 2(a).

2006; Xue et al. 2008; Wang, Miao, and Lu 2013). On the other hand, the wells W1, W2, W3, and W5 were not in the subsidence area after 2004 which may indicate that the consolidation of the strata around these wells was completed before 2004. The observations that there has been an upward rebound since 2004 in the area surrounding the wells W1, W2, W3, and W5 indicated that the strata at the wells W1, W2, W3, and W5 became uncompressed after 2004. With the rising of the groundwater, the stratum began to rebound.

We analysed correlations between the groundwater-table change and the surface deformation at six water well stations; the correlation between groundwater-table change and surface deformation indicates that the groundwater level was an important factor in affecting the surface deformation. However, other factors such as consolidation caused by surface loads due to infrastructures such as buildings, natural strata compression, and other geologic condition also contributed to land deformation (Wang et al. 2009; Zhang et al. 2010; Hu et al. 2009).

## 7. Conclusions

In this study, the C-band Envisat ASAR, L-band ALOS PALSAR, and X-band COSMO-SkyMed SAR data from 2006 to 2012 have been successfully used with the SBAS-

InSAR technique to investigate land deformation in Changzhou city, China. The comprehensive utilization of multi-band SAR data set delineated a long-term land deformation with more detailed information about surface deformation than single-band SAR data sets with less influenced by vegetation over a large area. The SBAS-InSAR method increased the utilization and quality of interferograms calculated from multi-band SAR data set and the powerful ability of this technique in the aspect of identify DS that were surrounded by completely decorrelated targets also help us get more detail information about land deformation. The InSAR results showed that several locations in Changzhou city, mainly distributed within the Wujin District, suffered serious subsidence, and the maximum subsidence rate reached as high as  $-58 \text{ mm year}^{-1}$ . Results from the multi-band SAR data sets showed that the subsidence in these regions was obvious and this subsiding trend may last for a while. The subsidence in these regions might be caused by the over-exploitation of groundwater and soil consolidation due to surface loading by artificial structures.

Cross-validation between the Envisat ASAR and ALOS PALSAR data showed that the Envisat ASAR and ALOS PALSAR measurements agreed well in general with  $r = 0.89$ . To assess the accuracy of the InSAR measurements, levelling observations at 11 locations were used. The comparison results between the InSAR and levelling measurements of surface deformation demonstrated that these two measurements were well correlated with  $r = 0.97$  and a standard deviation of 10.2 mm. They also indicated that the InSAR measurements agreed well with the ground-control data and can be used to provide deformation information about a much broader region around Changzhou city than the area covered by the small ground levelling network. The correlation analysis between the land deformation and the groundwater table at six groundwater wells showed that a sharp rise of groundwater level caused land rebound within the urban region (e.g. wells W1, W2, W3, and W5). However, subsidence was also observed along with simultaneous water-table rise (e.g. wells W4 and W6). This phenomenon was caused by the status of consolidation of the strata, especially the occurrence of creep features in the saturated sand layer.

In this study, we also discussed the influence of groundwater exploitation on surface subsidence and found that excessive exploitation of groundwater before 2000 was an important factor in land subsidence of Changzhou city. In the future, more data such as geological, human activities (such as constructing buildings) and other natural factors will be collected and used to confirm the mechanisms of land deformation.

## Acknowledgements

This work was supported by the Key Technology R&D Program of Jiangsu Province (BE2013702), programme for National Nature Science Foundation of China: [Grant Numbers 41371391, 41501497, and 41601497], and Jiangsu Graduate Student Research Innovative Projects: [Grant Number KYZZ16\_0046].

## Disclosure statement

No potential conflict of interest was reported by the authors..

## Funding

This work was supported by the National Natural Science Foundation of China: [Grant Numbers 41371391, 41501497, and 41601497], Jiangsu Provincial Bureau of Surveying Mapping and Geoinformation Research Project: [Grant Number JSCHKY201604], NUPTSF [Grant Number NY214195], Jiangsu Graduate Student Research Innovative Projects: [Grant Number KYZZ16\_0046], and Key Technology R&D Program of Jiangsu Province: [Grant Number BE2013702]

## References

- Abidin, H. Z., H. Andreas, I. Gumilar, T. P. Sidiq, and Y. Fukuda. 2013. "Land Subsidence in Coastal City of Semarang (Indonesia): Characteristics, Impacts and Causes." *Geomatics, Natural Hazards and Risk* 4 (3): 226–240. doi:10.1080/19475705.2012.692336.
- Akcin, H., H. S. Kutoglu, H. Kemaldere, T. Deguchi, and E. Koksal. 2010. "Monitoring Subsidence Effects in the Urban Area of Zonguldak Hardcoal Basin of Turkey by InSAR-GIS Integration." *Natural Hazards and Earth System Science* 10 (9): 1807–1814. doi:10.5194/nhess-10-1807-2010.
- Baek, J., S.-W. Kim, H.-J. Park, H.-S. Jung, K.-D. Kim, and J. W. Kim. 2008. "Analysis of Ground Subsidence in Coal Mining Area Using SAR Interferometry." *Geosciences Journal* 12 (3): 277–284. doi:10.1007/s12303-008-0028-3.
- Bayuaji, L., J. T. S. Sumantyo, and H. Kuze. 2010. "ALOS PALSAR D-InSAR for Land Subsidence Mapping in Jakarta, Indonesia." *Canadian Journal of Remote Sensing* 36 (1): 1–8. doi:10.5589/m10-023.
- Berardino, P., G. Fornaro, A. Fusco, D. Galluzzo, R. Lanari, E. Sansosti, and S. Usai. 2001. "A New Approach for Analyzing the Temporal Evolution of Earth Surface Deformations Based on the Combination of DIFSAR Interferograms." Paper presented at the IEEE International Geoscience and Remote Sensing Symposium, Sydney, 9–13 July 2001. IGARSS '01. doi:10.1109/IGARSS.2001.978085
- Berardino, P., G. Fornaro, R. Lanari, and E. Sansosti. 2002. "A New Algorithm for Surface Deformation Monitoring Based on Small Baseline Differential SAR Interferograms." *IEEE Transactions on Geoscience & Remote Sensing* 40 (11): 2375–2383. doi:10.1109/TGRS.2002.803792.
- Brunori, C., C. Bignami, M. Albano, F. Zucca, S. Samsonov, G. Groppelli, G. Norini, M. Saroli, and S. Stramondo. 2015. "Land Subsidence, Ground Fissures and Buried Faults: InSAR Monitoring of Ciudad Guzmán (Jalisco, Mexico)." *Remote Sensing* 7 (7): 8610–8630. doi:10.3390/rs70708610.
- Bürgmann, R., P. A. Rosen, and E. J. Fielding. 2000. "Synthetic Aperture Radar Interferometry to Measure Earth's Surface Topography and Its Deformation." *Annual Review of Earth & Planetary Sciences* 28: 169–209. doi:10.1146/annurev.earth.28.1.169.
- Costantini, M. 1998. "A Novel Phase Unwrapping Method Based on Network Programming." *IEEE Transactions on Geoscience & Remote Sensing* 36 (3): 813–821. doi:10.1109/36.673674.
- Dong, S., S. Samsonov, H. Yin, S. Ye, and Y. Cao. 2014. "Time-Series Analysis of Subsidence Associated with Rapid Urbanization in Shanghai, China Measured with SBAS InSAR Method." *Environmental Earth Sciences* 72 (3): 677–691. doi:10.1007/s12665-013-2990-y.
- Editor Board of Changzhou. 2009. *Changzhou's Yearbook*. Changzhou: Changzhou's Yearbook.
- Feng, Z. 2011. "Jiangsu: To Implement the Total Amount Control System and Make Scientific Use of Groundwater Resources." [In Chinese.] *Water Resource* 2011 (1): 66.
- Ferretti, A., A. Fumagalli, F. Novali, and C. Prati. 2011. "A New Algorithm for Processing Interferometric Data-Stacks: SqueeSAR." *IEEE Transactions on Geoscience & Remote Sensing* 49 (9): 3460–3470. doi:10.1109/TGRS.2011.2124465.

- Ferretti, A., C. Prati, and F. Rocca. 2000. "Nonlinear Subsidence Rate Estimation Using Permanent Scatterers in Differential SAR Interferometry." *IEEE Transactions on Geoscience & Remote Sensing* 38 (5): 2202–2212. doi:10.1109/36.868878.
- Ferretti, A., C. Prati, and F. Rocca. 2001. "Permanent Scatterers in SAR Interferometry." *IEEE Transactions on Geoscience & Remote Sensing* 39 (1): 8–20. doi:10.1109/36.898661.
- Ferretti, A., G. Savio, R. Barzaghi, and A. Borghi. 2007. "Submillimeter Accuracy of InSAR Time Series: Experimental Validation." *IEEE Transactions on Geoscience & Remote Sensing* 45 (5): 1142–1153. doi:10.1109/TGRS.2007.894440.
- Ge, L., A. H.-M. Ng, X. Li, H. Z. Abidin, and I. Gumilar. 2014. "Land Subsidence Characteristics of Bandung Basin as Revealed by ENVISAT ASAR and ALOS PALSAR Interferometry." *Remote Sensing of Environment* 154: 46–60. doi:10.1016/j.rse.2014.08.004.
- Hallegatte, S., C. Green, R. J. Nicholls, and J. Corfee-Morlot. 2013. "Future Flood Losses in Major Coastal Cities." *Nature Climate Change* 3 (9): 802–806. doi:10.1038/nclimate1979.
- Hooper, A. J. 2006. "Persistent scatter radar interferometry for crustal deformation studies and modeling of volcanic deformation." PHD diss., Stanford University.
- Hu, J. 2011. "A Study on the Land Subsidence Effect after Prohibiting Extraction of Groundwater in Suzhou-Wuxi-Changzhou Area." PHD diss., Nanjing University.
- Hu, J., B. Shi, H. I. Inyang, J. Chen, and Z. Sui. 2009. "Patterns of Subsidence in the Lower Yangtze Delta of China: The Case of the Suzhou-Wuxi-Changzhou Region." *Environ Monit Assess* 153 (1–4): 61–72. doi:10.1007/s10661-008-0336-0.
- Hu, J., Z.-W. Li, J. Li, L. Zhang, X.-L. Ding, J.-J. Zhu, and Q. Sun. 2014. "3-D Movement Mapping of the Alpine Glacier in Qinghai-Tibetan Plateau by Integrating D-InSAR, MAI and Offset-Tracking: Case Study of the Dongkemadi Glacier." *Global and Planetary Change* 118: 62–68. doi:10.1016/j.gloplacha.2014.04.002.
- Jiang, M., Z. W. Li, X. L. Ding, J. J. Zhu, and G. C. Feng. 2011. "Modeling Minimum and Maximum Detectable Deformation Gradients of Interferometric SAR Measurements." *International Journal of Applied Earth Observation & Geoinformation* 13 (5): 766–777. doi:10.1016/j.jag.2011.05.007.
- Kampes, B. 2006. *Radar Interferometry – Persistent Scatterer Technique*. New York: Springer.
- Kim, J.-W., Z. Lu, Y. Jia, and C. K. Shum. 2015. "Ground Subsidence in Tucson, Arizona, Monitored by Time-Series Analysis Using Multi-Sensor InSAR Datasets from 1993 to 2011." *ISPRS Journal of Photogrammetry and Remote Sensing* 107: 126–141. doi:10.1016/j.isprsjprs.2015.03.013.
- Kim, S. W., S. Wdowinski, T. H. Dixon, F. Amelung, J. S. Won, and J. W. Kim. 2008. "InSAR-based Mapping of Surface Subsidence in Mokpo City, Korea, Using JERS-1 and ENVISAT SAR Data." *Earth, Planets and Space* 60 (5): 453–461. doi:10.1186/BF03352812.
- Lanari, R., F. Casu, M. Manzo, G. Zeni, P. Berardino, M. Manunta, and A. Pepe. 2007. "An Overview of the Small Baseline Subset Algorithm: A DInSAR Technique for Surface Deformation Analysis." *Pure and Applied Geophysics* 164 (4): 637–661. doi:10.1007/s00024-007-0192-9.
- Lanari, R., O. Mora, M. Manunta, and J. J. Mallorqui. 2004. "A Small-Baseline Approach for Investigating Deformations on Full-Resolution Differential SAR Interferograms." *IEEE Transactions on Geoscience & Remote Sensing* 42 (7): 1377–1386. doi:10.1109/TGRS.2004.828196.
- Li, W., and J. Wu. 2015. "Research on Monitoring Method System of Land Subsidence in Suzhou-Wuxi-Changzhou Area." [In Chinese.] *Global Geology* 34 (3): 862–869.
- Li, Z. W., Z. F. Yang, J. J. Zhu, J. Hu, Y. J. Wang, P. X. Li, and G. L. Chen. 2015. "Retrieving Three-Dimensional Displacement Fields of Mining Areas from a Single InSAR Pair." *Journal of Geodesy* 89 (1): 17–32. doi:10.1007/s00190-014-0757-1.
- Liao, M., J. Tang, T. Wang, T. Balz, and L. Zhang. 2012. "Landslide Monitoring with High-Resolution SAR Data in the Three Gorges Region." *Science China Earth Sciences* 55 (4): 590–601. doi:10.1007/s11430-011-4259-1.
- Ma, F. S., Y. S. Yang, R. M. Yuan, B. K. Yao, and J. Guo. 2011. "Effect of Regional Land Subsidence on Engineering Structures: A Case Study of the 6 Km Long Su-Tong Yantze River Bridge." *Bulletin of Engineering Geology and the Environment* 70 (3): 449–459. doi:10.1007/s10064-010-0336-5.
- Meng, H. 2011. "The analysis of the large-scale city buildings loads on land subsidence." MA diss., Chang'an University.

- Miao, X. T., X. X. Zhu, M.-L. Lu, F. C. Chen, and A.-F. Huangfu. 2007. "Groundwater Exploration from the Confined Aquiferous II and Land Subsidence Control of Suxichang Area." [In Chinese.] *Chinese Journal of Geological Hazard & Control* 18 (2): 132–139.
- Perissin, D., and T. Wang. 2011. "Time-Series InSAR Applications over Urban Areas in China." *IEEE Journal of Selected Topics in Applied Earth Observations & Remote Sensing* 4 (1): 92–100. doi:10.1109/JSTARS.2010.2046883.
- Qin, Y., and D. Perissin. 2015. "Monitoring Ground Subsidence in Hong Kong via Spaceborne Radar: Experiments and Validation." *Remote Sensing* 7 (8): 10715–10736. doi:10.3390/rs70810715.
- Qu, F., Q. Zhang, Z. Lu, C. Zhao, C. Yang, and J. Zhang. 2014. "Land Subsidence and Ground Fissures in Xi'an, China 2005–2012 Revealed by Multi-Band InSAR Time-Series Analysis." *Remote Sensing of Environment* 155: 366–376. doi:10.1016/j.rse.2014.09.008.
- Scharroo, R., and P. Visser. 1998. "Precise Orbit Determination and Gravity Field Improvement for the ERS Satellites." *Journal of Geophysical Research: Oceans* 103 (C4): 8113–8127. doi:10.1029/97JC03179.
- Shi, X., J. Wu, S. Ye, Y. Zhang, Y. Xue, Z. Wei, Q. Li, and J. Yu. 2008. "Regional Land Subsidence Simulation in Su-Xi-Chang Area and Shanghai City, China." *Engineering Geology* 100 (1–2): 27–42. doi:10.1016/j.enggeo.2008.02.011.
- Shi, X., R. Fang, J. Wu, H. Xu, Y. Sun, and J. Yu. 2012. "Sustainable Development and Utilization of Groundwater Resources considering Land Subsidence in Suzhou, China." *Engineering Geology* 124: 77–89. doi:10.1016/j.enggeo.2011.10.005.
- Shi, X., Y. Xue, J. Wu, Y. Zhang, J. Yu, and J. Zhu. 2006. "A Study of Soil Deformation Properties of the Groundwater System in the Changzhou Area." [In Chinese.] *Hydrogeology & Engineering Geology* 3:1–6.
- Tomiyama, N., K. Koike, and M. Omura. 2004. "Detection of Topographic Changes Associated with Volcanic Activities of Mt. Hoshho Using D-InSAR." *Advances in Space Research* 33 (3): 279–283. doi:10.1016/S0273-1177(03)00483-6.
- Tung, H., and J. C. Hu. 2012. "Assessments of Serious Anthropogenic Land Subsidence in Yunlin County of Central Taiwan from 1996 to 1999 by Persistent Scatterers InSAR." *Tectonophysics* 578: 126–135. doi:10.1016/j.tecto.2012.08.009.
- Wang, F., L. Miao, and W. Lu. 2013. "Sand Creep as a Factor in Land Subsidence during Groundwater Level Recovery in the Southern Yangtze River Delta, China." *Bulletin of Engineering Geology and the Environment* 72 (3–4): 273–283. doi:10.1007/s10064-013-0474-7.
- Wang, G., M. Xie, X. Chai, L. Wang, and C. Dong. 2013. "D-InSAR-based Landslide Location and Monitoring at Wudongde Hydropower Reservoir in China." *Environmental Earth Sciences* 69 (8): 2763–2777. doi:10.1007/s12665-012-2097-x.
- Wang, G. Y., G. You, B. Shi, J. Yu, and M. Tuck. 2009. "Long-Term Land Subsidence and Strata Compression in Changzhou, China." *Engineering Geology* 104 (1–2): 109–118. doi:10.1016/j.enggeo.2008.09.001.
- Wang, R., Y. Xia, H. Grosser, H.-U. Wetzell, H. Kaufmann, and J. Zschau. 2004. "The 2003 Bam (SE Iran) Earthquake: Precise Source Parameters from Satellite Radar Interferometry." *Geophysical Journal International* 159 (3): 917–922. doi:10.1111/gji.2004.159.issue-3.
- Wu, J., S. Wu, M. Wang, and W. Li. 2014. "Review on Recent Progress of Land Subsidence Control in Suzhou-wuxi-changzhou Area." [In Chinese.] *Journal of Geology* 38 (2): 319–323. doi:10.3969/j.issn.1674-3636.2014.02.319.
- Xie, Y., N. Cao, and L. Xu. 2009. "Land Subsidence Monitoring in Changzhou." [In Chinese.] *City Urban Geotechnical Investigation & Surveying* 6:103–105.
- Xu, H., Z. Zhou, and Z. Gao. 2011a. "Experimental Study on Coefficient of Consolidation of Land Subsidence." [In Chinese.] *Chinese Journal of Geotechnical Engineering* 33 (12): 1969–1973.
- Xu, H., Z. Zhou, and Z. Gao. 2011b. "Experimental Research of Hysteresis Effect of Land Subsidence Caused by Water Releasing." [In Chinese.] *Chinese Journal of Rock Mechanics and Engineering* 30 (s2): 3595–3601.
- Xu, Y.-S., L. Ma, Y.-J. Du, and S.-L. Shen. 2012. "Analysis of Urbanisation-Induced Land Subsidence in Shanghai." *Natural Hazards* 63 (2): 1255–1267. doi:10.1007/s11069-012-0220-7.

- Xu, Y.-S., Y. Yuan, S.-L. Shen, Z.-Y. Yin, H.-N. Wu, and L. Ma. 2015. "Investigation into Subsidence Hazards Due to Groundwater Pumping from Aquifer II in Changzhou, China." *Natural Hazards* 78 (1): 281–296. doi:10.1007/s11069-015-1714-x.
- Xue, Y., J. Wu, Y. Zhang, S. Ye, X. Shi, Z. Wei, A. Q. Li, and J. Yu. 2008. "Simulation of Regional Land Subsidence in the Southern Yangtze Delta." *Science in China Series D: Earth Sciences* 51 (6): 808–825. doi:10.1007/s11430-008-0062-z.
- Yin, H. 2013. *English for Geomatics Engineering*. Wuhan: Wuhan University Press.
- Yin, J., D. Yu, and R. Wilby. 2016. "Modelling the Impact of Land Subsidence on Urban Pluvial Flooding: A Case Study of Downtown Shanghai, China." *Science of the Total Environment* 544: 744–753. doi:10.1016/j.scitotenv.2015.11.159.
- Zhang, Y., J. Zhang, H. Wu, Z. Lu, and S. Guangtong. 2011. "Monitoring of Urban Subsidence with SAR Interferometric Point Target Analysis: A Case Study in Suzhou, China." *International Journal of Applied Earth Observation and Geoinformation* 13 (5): 812–818. doi:10.1016/j.jag.2011.05.003.
- Zhang, Y., Y.-Q. Xue, J.-C. Wu, S.-J. Ye, Z.-X. Wei, Q.-F. Li, and J. Yu. 2007. "Characteristics of Aquifer System Deformation in the Southern Yangtze Delta, China." *Engineering Geology* 90 (3–4): 160–173. doi:10.1016/j.enggeo.2007.01.004.
- Zhang, Y., Y.-Q. Xue, J.-C. Wu, X.-Q. Shi, and J. Yu. 2010. "Excessive Groundwater Withdrawal and Resultant Land Subsidence in the Su-Xi-Chang Area, China." *Environmental Earth Sciences* 61 (6): 1135–1143. doi:10.1007/s12665-009-0433-6.
- Zhu, W., and F. Liu. 2007. "Surface Subsidence Observation and Results Analysis of Changzhou, China." [In Chinese.] *Engineering of Surveying and Mapping* 16 (6): 54–57.